EPJ Web of Conferences **164**, 01021 (2017) DOI: 10.1051/epjconf/201716401021
ICNFP 2016

Performance of the ATLAS Detector in Run-2

Nicoletta Garelli[1,a] on behalf of the ATLAS Collaboration

[1] *SLAC National Accelerator Laboratory, 2575 Sand Hill Rd, Menlo Park, CA 94025, United States*

Abstract. The second LHC run has started in June 2015 with a p-p center-of-mass collision energy of 13 TeV and ATLAS has taken 3.2 fb^{-1} of data at the new energy in 2015. In this talk the improvements made to the ATLAS experiment during the two-year shutdown 2013/2014 will be discussed. Furthermore, reconstruction algorithms of tracks, e/γ, muons, taus, jets and flavour tagging have been improved for Run-2. Reconstruction efficiency, isolation performance, transverse momentum resolution and momentum scales are measured in various regions of the detector and in momentum intervals enlarged with respect to those measured in the Run-1. The performance of the upgraded detector and the new reconstruction algorithms measured using these data taken in 2015 will be discussed.

1 Introduction

The second three-year run of the Large Hadron Collider (LHC) marks a new era for high energy physics. More data are needed in order to assess the nature of the Higgs boson observed in 2012 with the ATLAS experiment, while the existence of dark matter and unnatural fine tuning in the Standard Model also motivate potential new physics near the electroweak energy scale. The discovery of the Higgs boson with mass $126.0 \pm 0.4(stat) \pm 0.4(sys)$ GeV is detailed here [1]; the searches have been performed in three channels: $H \to ZZ^{(\star)} \to 4l$, $H \to \gamma\gamma$ and $H \to WW^{(\star)} \to e\nu\mu\nu$.

The LHC took two years of shutdown from February 2013, referred to as Long Shutdown 1, for upgrading the machine to reach a center of mass energy of 13 TeV and peek luminosity up to $1.5 \cdot 10^{34}$ $cm^{-2}s^{-1}$, beyond original design, operating with a bunch spacing of 25 ns. The experiments took advantage from this time to repair broken components, update their online systems and install new detector components to cope with the upgraded LHC and the expected pile-up (μ) of about 40.

2 The ATLAS Detector

A Toroidal LHC Apparatus (ATLAS) is a general purpose detector at the LHC installed at Point 1 of the accelerator ring [2]. It has a forward-backward symmetry which provides almost full solid angle coverage around the interaction point [1]. ATLAS is a big cylinder weighing 7000 t, 44 m long and 22 m high, composed of an inner tracker, a calorimeter system and a muon spectrometer. The Inner Detector

[a] e-mail: nicoletta.garelli@cern.ch

[1] ATLAS uses a right-handed coordinate system with its origin at the nominal interaction point (IP) in the center of the detector and the z-axis along the beam pipe. The x-axis points from the IP to the center of the LHC ring, and the y-axis points upwards. Cylindrical coordinates (r, ϕ) are used in the transverse plane, ϕ being the azimuthal angle around the z-axis. The pseudo-rapidity is defined in terms of the polar angle θ as $\eta = -ln(tan\frac{\theta}{2})$.

(ID) is surrounded by a superconducting solenoid providing a 2 T axial magnetic field. It consists of silicon pixels and the SemiConductor Tracker (SCT) built from silicon strips, with pseudo-rapidity coverage up to $|\eta| = 2.5$ and a gas filled straw tubes detector, the Transition Radiation Tracker (TRT), with pseudo-rapidity coverage up to $|\eta| = 2$. The calorimeter system surrounds the solenoid. Showers produced by photons, electrons and positrons are contained in the electromagnetic calorimeter (EM) which uses liquid argon as active medium. The hadronic showers are adsorbed by the Tile calorimeter in the barrel and more liquid argon calorimeter in the endcaps. The calorimeter detectors cover the pseudo-rapidity range of $|\eta| < 4.9$. The muon spectrometer is composed of precision measurement chambers and trigger chambers located within three super-conducting toroids arranged with an eight-fold azimuthal symmetry, covering $|\eta| < 2.7$. The toroidal magnetic field in the barrel region is 0.5 T, while in the end-caps 1 T.

2.1 Major ATLAS Activities during the LS1

ATLAS underwent a series of updates to cope with the new LHC working point for Run-2. The most significant ones are summarized below.

The pixel detector was extracted and equipped on surface with new services. A fourth additional layer, referred to as Insertable B-Layer (IBL) was added between a new beam pipe and the current inner pixel layer (B-layer) to improve the *b*-tagging efficiency and helping preserving tracking performance in face of higher luminosity effects. It is installed at 33 mm from the beam line and equipped with planar and 3D sensors [3].

During the Run-1, significant TRT gas leaks were observed, and many repaired during the LS1. For regions not fully repaired, it has been decided to switch to an argon based gas mixture instead of mitigate the unaffordable xenon loss.

New muon detector chambers were installed to close the coverage holes both in the feet region and in the shafts area where elevators are located to lift material from the ground level up to below the calorimeter systems.

A new off-detector readout complex was deployed for the Cathode Strip Chambers (CSC) to remove the previous limitations to sustain 100 kHz level-1 trigger rate. It is the first ATCA-based system of the ATLAS experiment and worked very reliably from the beginning of operations in 2015 [4].

All the accessible front-ends were repaired to improve the overall ATLAS efficiency reaching more than 96% of operational fraction across all detector systems prior to the start of the Run-2.

2.1.1 Consolidation Work during the YETS 2015

The Year-End-Technical-Stop (YETS) of 2015 lasted few months. The most significant ATLAS task during this shutdown was the repair of the two vacuum bellows in one of the endcap toroid cryostats. A damage was in fact discovered around the leads of the endcap toroid C, and the repair was carefully prepared and completed on time.

3 The ATLAS Performance

On 3 June 2015 the LHC delivered the first collisions at 13 TeV, after two months of beam commissioning. The rest of the year was characterized by a step-wise increase in the number of bunches that allowed to reach a peak luminosity of $5 \cdot 10^{33}\,\mathrm{cm}^{-2}\mathrm{s}^{-1}$, although still below the maximum value of Run-1 ($7.7 \cdot 10^{33}\,\mathrm{cm}^{-2}\mathrm{s}^{-1}$). The luminosity performance was excellent, thanks to the small beam losses and good emittance preservation through the beam cycle. In 2016 the peak luminosity exceeded the

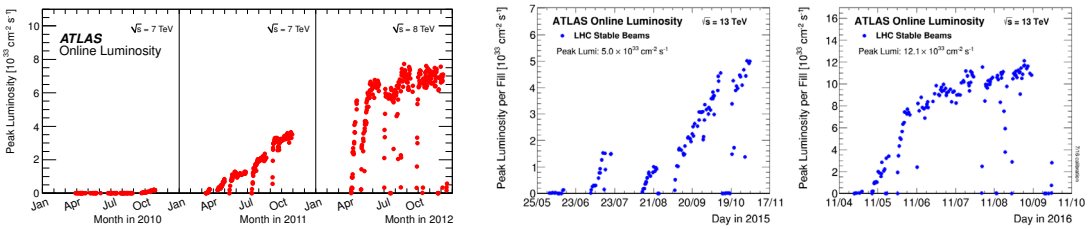

Figure 1: The peak instantaneous luminosity delivered to ATLAS per day versus time during stable beams for p-p collisions in 2010, 2011 and 2012 (*left*) [5], in 2015 (*center*), and in 2016 (*right*) [6].

nominal value of $1 \cdot 10^{34}\,\mathrm{cm}^{-2}\mathrm{s}^{-1}$ by early summer, and reached up to $1.2 \cdot 10^{34}\,\mathrm{cm}^{-2}\mathrm{s}^{-1}$ in September, as shown in figure 1.

The luminosity integrated by ATLAS over the course of 2015 p-p runs was above $4\,\mathrm{fb}^{-1}$ with an average pile-up of about 14, while between 16 April and 25 July of 2016 ATLAS collected over $18\,\mathrm{fb}^{-1}$ with an average pile-up of about 23, as reported in figure 2. The luminosity is determined from luminosity detectors which have been calibrated with the use of the van-der-Meer beam-separation method.

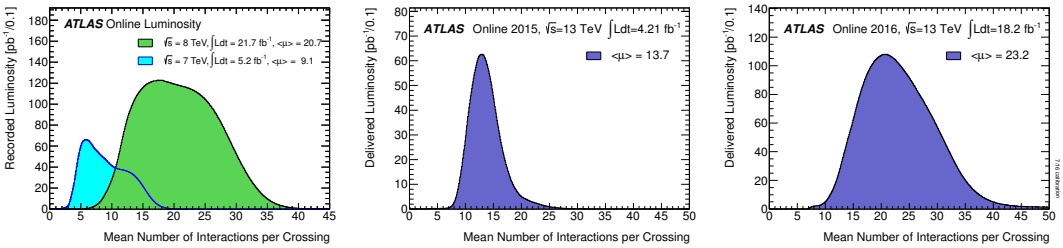

Figure 2: The luminosity-weighted distribution of the mean number of interactions per crossing for the 2011 and 2012 data (*left*), the 2015 (*center*) [5], and the 16 April to 25 July 2016 (*right*) p-p collision data [6]. All data delivered to ATLAS during stable beams is shown, and the integrated luminosity and the mean pile-up (μ) values are given in the plots.

The ratio between the luminosity recorded by ATLAS and the total delivered luminosity establishes the data taking efficiency. In 2012 it was 93.5%, while in 2015 and between April and September 2016 it was 92%.

The data quality efficiency instead takes into account the relative detector uptime and good data quality efficiency during stable beam pp collisions. The data quality efficiency in the 2015 25ns bunch spacing p-p runs was 87.1%. The two long LHC fills where IBL was turned off, as reported in section 3.1, significantly contributed to the lower efficiency with respect to the 95.5% value of Run-1.

In the following sections the status of the ATLAS detector, the performance of the reconstruction of the main physics objects and the efficiency measurements in 2015 are summarized.

3.1 IBL Commissioning

During the cosmic ray commissioning of the IBL in early 2015 a mechanical distortion of its support structure, the staves, was observed. The bowing of the staves depends linearly on the temperature with a gradient of about 10 μm/K twisting the staves in the r-ϕ direction. The impact of this effect is mitigated by a temperature control to 0.2 K level [7].

For two LHC fills in October 2015 the IBL was off and excluded by the ATLAS data taking due to the observation of a significant front-end low voltage current increase and drift in the calibration parameters (the threshold and the time over threshold). This effect is compatible with the front-end radiation damage which was initially somewhat surprising given the FE ASIC design was qualified for about 100 times the dose at that point. This was soon understood to be similar to several other observations of a transient effect related to typical designs also on 130νm technologies and the current is expected to decrease after about 1 Mrad dose [8].

After the observations in 2015, it was decided to run IBL at 15 °C in early 2016 instead of the nominal −10 °C, and at the decreased digital voltage of 1 V. After measurements in the laboratories, in the summer it was decided to reduce the temperature to 5 °C and increase the voltage back to 1.2 V. IBL accumulated so far about 9 Mrad and the observed current has significantly reduced from the maximum peak. Figure 3 compares the correction needed for the IBL distortion in the three different temperature settings. The effects are regularly corrected online before the reconstruction of the data. After applying the alignment correction, they do not impact the tracking performance significantly.

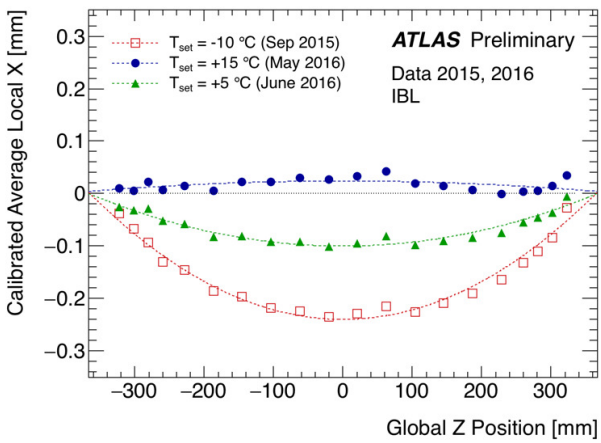

Figure 3. IBL local-x correction in the transverse plane averaged over all 14 IBL staves for 2015 data (*red open squares*), and for 2016 data at different operating temperatures (15 °C, *solid blue circles*; 5 °C, *solid green triangles*) [9].

The IBL is composed of twelve million pixel cells of $50 \times 250\,\mu\text{m}^2$ versus $50 \times 400\,\mu\text{m}^2$ for the original pixel detector. The smaller size in the z-direction results in an improved Z spatial resolution of 40 μm instead of 75 μm. Figure 4 shows the improved resolution of the impact parameter with respect to 2012. At low p_T both d_0 and z_0 resolution improve close to a factor of two because of the IBL addition so close to the interaction point and lighter stave material reducing the impact of multiple scattering. At high p_T, where the detector granularity dominates, the improved resolution is only in the longitudinal impact parameter due to the IBL pixel size.

3.2 ID Tracking Performance

Tracks above a certain p_T threshold are reconstructed offline with the full acceptance range of the ID, with multi-stage track identification algorithms. The inside-out algorithm reconstructs mostly

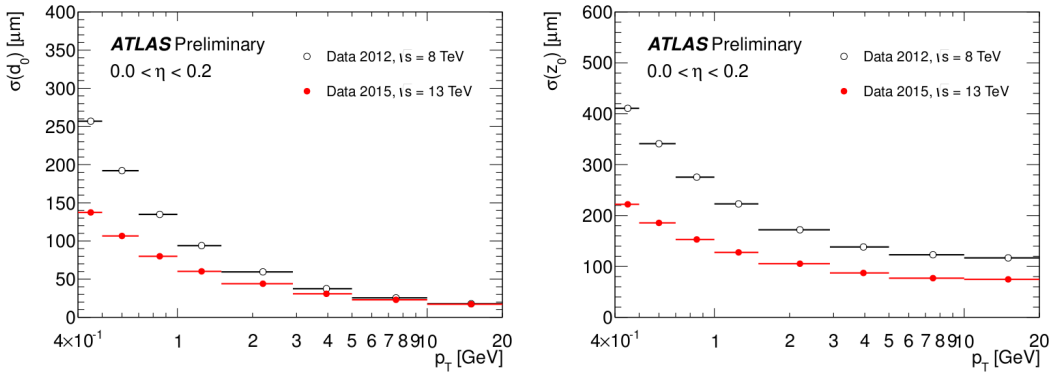

Figure 4: Comparison of the impact parameter resolution in Run-1 (black empty circles) and 2015 (red filled circles). [10]

particles produced in the primary p-p collisions. The tracks are seeded in the pixel detector (three seeds) and the hits from the neighboring SCT layers are added. The track candidates found in the silicon detectors are then extrapolated to include measurements in the TRT.

The outside-in algorithm starts from segments reconstructed in the TRT and extends them inwards by adding silicon hits not yet used by inside-out tracking. It reconstructs secondary charged tracks (*e.g.* photon conversions, material interactions).

Reconstructed tracks are selected by applying quality criteria for typical physics analyses. The *Loose* tracks have $|p_T| > 400\,\text{MeV}$, $|\eta| < 2.5$, number of silicon hits ≥7, number of shared modules ≤1, number of silicon holes ≤2, number of pixel holes ≤1. The *Tight Primary* tracks, in addition to the *Loose* selection requirements have number of silicon hits ≥9 if $|\eta| \leq 1.65$, number of silicon hits ≥11 if $|\eta| \leq 1.65$, at least one hit on the two innermost pixel layers, and no pixel holes.

The tracking efficiency for primary tracks in 2015 for tracks above 5 GeV remained high, as shown in figure 5: 90% for Loose and 85% for Tight Primary selections [11].

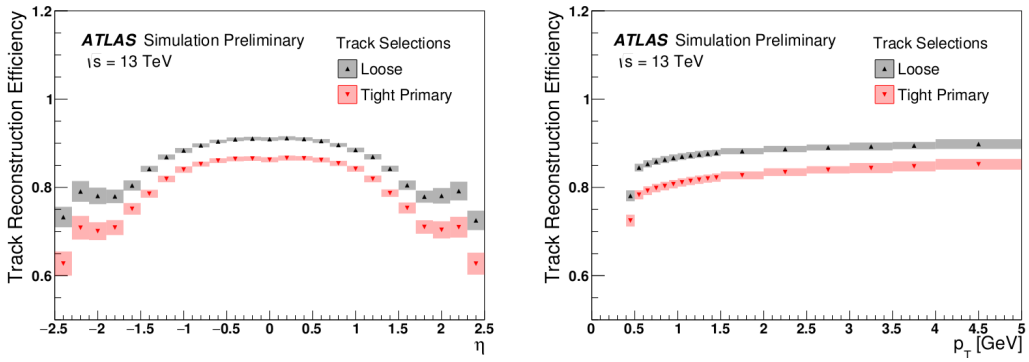

Figure 5: Track reconstruction efficiency in 2015 [11].

3.3 *b*-tagging Performance

The identification of b-quark jets plays a crucial role for the Run-2 measurements, both within the Standard Model and the New Physics scenarios. The addition of the IBL and the several enhancements to the tracking and the b-tagging algorithms significantly improve the performance, as illustrated in [12]. Figure 6 shows the comparison between the performance of the default b-tagging algorithm for Run-1 (MV1c) and the default one of Run-2 (MV2c20). Comparing the two algorithms, the light-flavour jet rejection is improved by a factor of about 4 and the c-jet rejection by a factor of between 1.5-2 for a 70% b-jet efficiency.

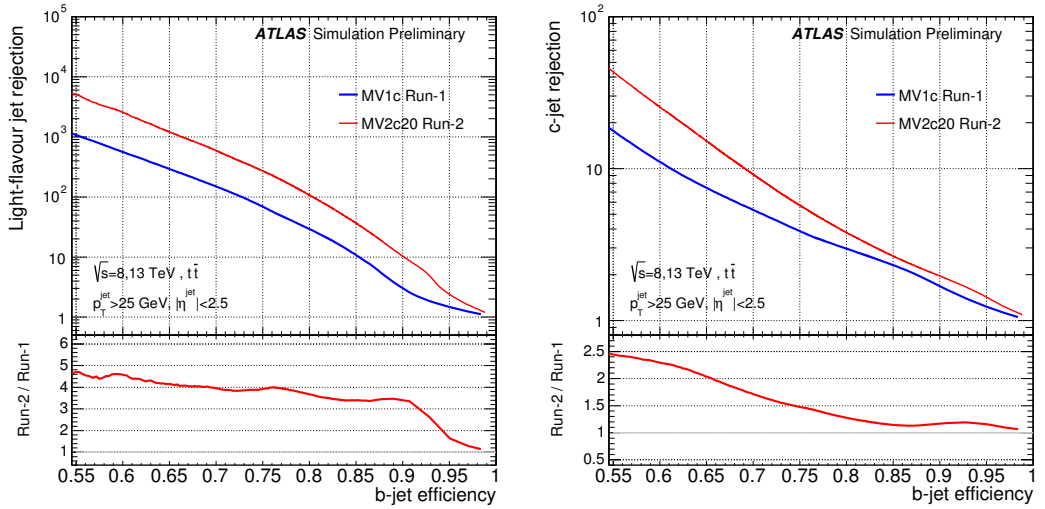

Figure 6: The light (*left*) and c-jet rejection (*right*) versus b-jet efficiency for the Run-1 detector and reconstruction software (blue) compared to algorithm using the Run-2 setup (red) [12].

3.4 Jet Reconstruction Performance

Nearly all the LHC physics arise from quark and gluon interactions, thus a detailed understanding of the quantum chromodinamics (QCD) is fundamental for analyzing new interesting phenomena and their background. Precision measurements of the production of jets are crucial tests of QCD.

The details of the ATLAS jet calibration in 2015 can be found here [13]. To cluster particles belonging to the same jet, the anti$-k_t$ algorithm with radius parameter $R = 0.4$ is used. The input is the positive-energy topological clusters (topoclusters) of the calorimeter cell energies. The uncertainty of the jet energy scale is the dominant experimental uncertainty and an estimate can be derived by in situ measurements. The first in situ results of the jet energy scale using the p-p 13 TeV dataset of 2015, approximately 3.3 fb^{-1} of data, show an agreement between data and Monte Carlo better than 2% up to 3 TeV, as seen in Figure 7. The analog signals of the EM calorimeter are sampled digitally once per bunch crossing over four bunch crossings and those measurements are converted to an energy measurement using constants calculated using dedicated calibration runs. During Run-1, five samples instead of four were used. Noise-levels defined for the calibration of the topoclustering algorithm in 2015 have changed with respect to Run-1 in order to better match noise measurements made in 2012 data.

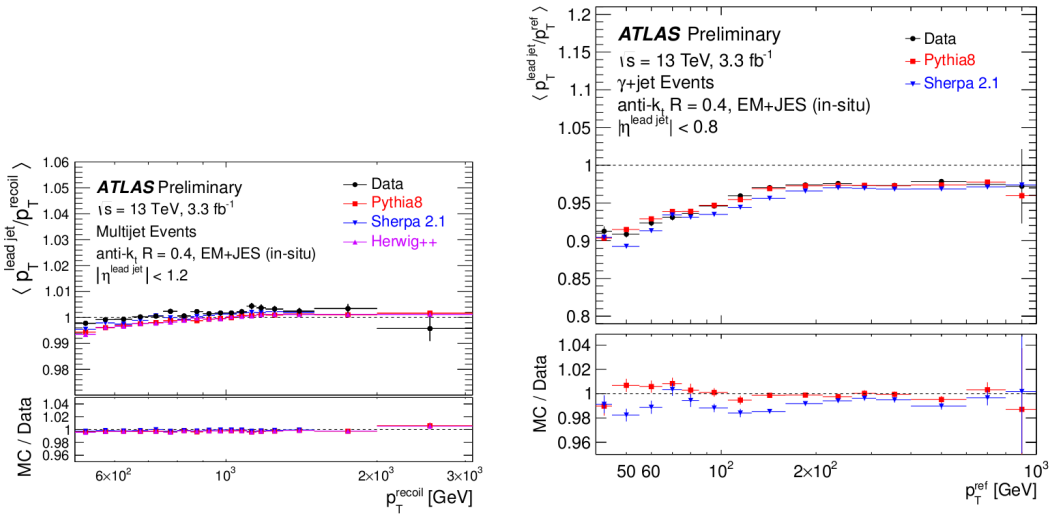

Figure 7: Multijet balance validation (*left*) and γ plus jet balance validation (*right*) in 13 TeV data and MC simulation [14].

3.5 e/γ Reconstruction Performance

Electrons and photons are excellent probes for interesting signatures in p-p collisions, including the Standard Model Higgs decay channel $H \to \gamma\gamma$.

The ATLAS electron efficiency measurements in 2015 are detailed in [15]. The electron identification is based on a likelihood combining the electromagnetic calorimeter showers, tracking, track-cluster matching and TRT particle-identification to separate isolated electrons. Several changes to the input variables used for the electron identification have been introduced in Run-2. In particular, the number of IBL hits is used for discriminating between electrons and converted photons, and new discriminating variables in the algorithms have been used due to the change in the TRT gas. The reconstruction efficiency is comparable to the one observed in 2012. The combined reconstruction and identification efficiency in $Z \to ee$ events are shown in Figure 8.

The identification of prompt photons relies on the high granularity of the calorimeter system. Three independent methods have been exploited to identify photons with the 2015 p-p collisions data. At low energy radiative photons from $Z \to ll\gamma$ are used; in the medium energy range shower shape properties of electrons from $Z \to ee$ decays are extracted and extrapolated to photons; while at high energy the efficiency on samples of reconstructed photons is directly measured after subtracting the hadronic background with a technique based on track isolation. The identification efficiency measurements are detailed in [16] and a comparison of the data driven measurements of the identification efficiency for unconverted photons is shown in Figure 8. The photon identification efficiency increases from 53−64% (47−61%) for unconverted (converted) photons at $E_T \sim 10$ GeV to 88−92% (96−98%) for $E_T \geq 100$ GeV.

3.6 Tau Reconstruction Performance

The tau leptons play an important role in the Higgs physics and new physics searches, and in the detector performance studies such as the transverse missing energy determination. The hadronically

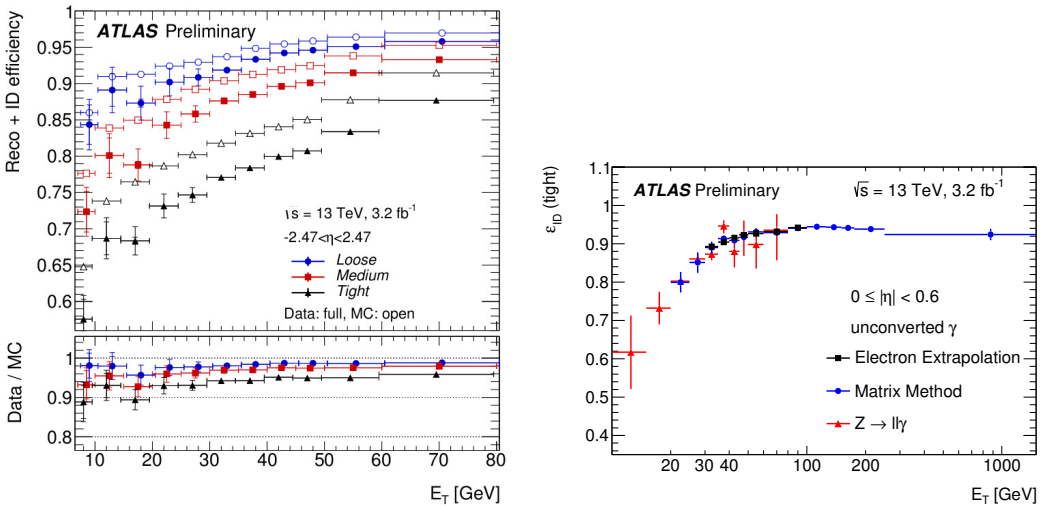

Figure 8: Combined electron reconstruction and identification efficiency in $Z \to ee$ events as a function of the transverse energy E_T (*left*) [15]. Comparison of the data-driven measurements of the identification efficiency for unconverted photons (*right*) [16].

decaying taus are narrow jets with low track multiplicity. They are identified using boosted decision tree to distinguish them from other jets and the performance is evaluated using $Z \to \tau\tau$ candidates.

A good agreement between data and simulation both in 2015 and 2016 is registered, as shown in Figure 9 and described in [17].

3.7 Muon System Performance

The ATLAS muon spectrometer performed very well during Run 2, with an alignment precision of about 50 μm for both barrel and endcap.

The reconstruction of the muons is crucial to some of the most important physics results published by ATLAS. This article [19] describes the performance of the ATLAS muon reconstruction measured using 3.2 fb^{-1} of data in 2015. The calibration sample consists of $Z \to \mu\mu$ decays and $J/\Psi \to \mu\mu$ decays. The dimuon invariant mass distributions are shown in figure 10. The muon reconstruction efficiency is measured to be close to 99% over most of the covered phase space ($|\eta| < 2.5$ and $5 < p_T < 100$ GeV). The isolation efficiency varies between 93% and 100% depending on the selection applied and on the momentum of the muon. The p_T resolution in data and simulation agree to better than 5% for most of the η range.

4 Conclusion

ATLAS underwent several upgrades during the two-year shutdown 2013/2014 referred to as LS1. The restart after the LS1 and the data taking through-out 2015 has been very successful. Despite the challenging conditions, the system stability and the data taking efficiency have quickly reached the Run-1 level. Detailed performance studies demonstrate good understanding of the 2015 data. The 2016 data taking started on 25 April, with an excellent LHC performance, an integrated luminosity in

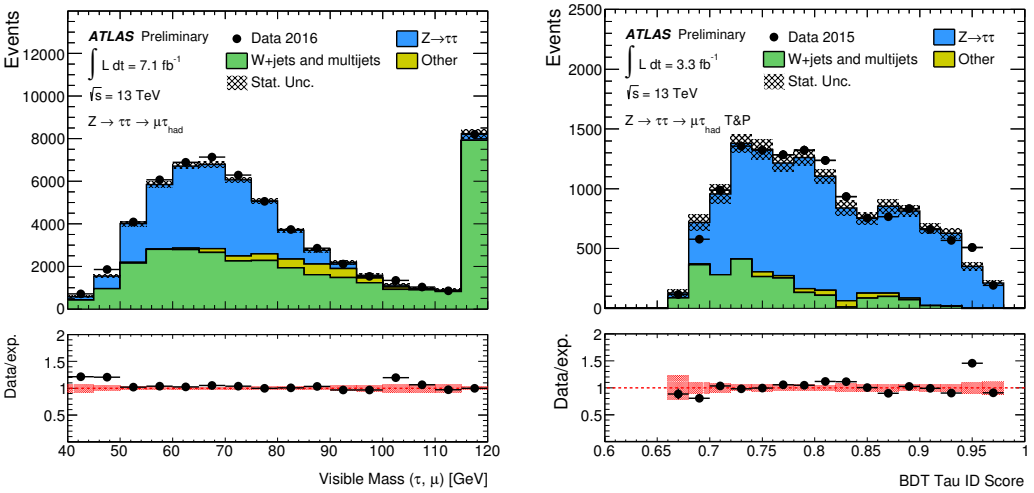

Figure 9: The visible mass reconstructed using isolated muons and offline tau candidates passing the offline loose identification requirement (*left*). The BDT tau identification score for offline tau candidates passing the offline medium identification requirement (*right*) [18].

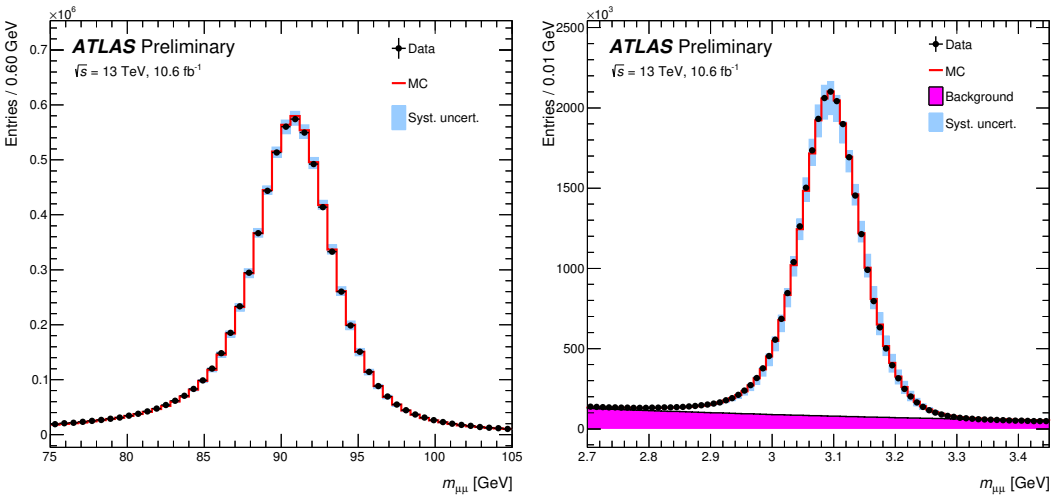

Figure 10: Dimuon invariant mass distribution of $Z \to \mu\mu$ events (*left*) and $J/\Psi \to \mu\mu$ events (*right*) reconstructed with combined muons. The points show the data. The continuous line corresponds to the simulation with the momentum corrections applied. Simulations are normalized to data [19].

early summer already higher than in 2015, and the instantaneous luminosity beyond the design level of $1 \cdot 10^{34}\,\mathrm{cm}^{-2}\mathrm{s}^{-1}$.

References

[1] The ATLAS Collaboration, Physics Letters B **Volume 716, Issue 1**, pages 1-29 (2012)
[2] The ATLAS Collaboration, JINST 3 **S08003**, (2008)
[3] Capeans, M. et al., *ATLAS Insertable B-Layer Technical Design Report* (2010)
[4] The ATLAS Collaboration, ATL-MUON-PROC-2015-009 (2015)
[5] https://twiki.cern.ch/twiki/bin/view/AtlasPublic/LuminosityPublicResults
[6] https://twiki.cern.ch/twiki/bin/view/AtlasPublic/LuminosityPublicResultsRun2
[7] The ATLAS Collaboration, ATL-INDET-PUB-2015-001 (2015)
[8] F. Faccio, G. Cervelli, IEEE Transactions on Nuclear Science **Volume 52, Issue 6**, pages 2413-2420 (2005)
[9] https://atlas.web.cern.ch/Atlas/GROUPS/PHYSICS/PLOTS/IDTR-2016-005
[10] https://atlas.web.cern.ch/Atlas/GROUPS/PHYSICS/PLOTS/IDTR-2015-007
[11] The ATLAS collaboration, ATL-PHYS-PUB-2015-051 (2015)
[12] The ATLAS collaboration, ATL-PHYS-PUB-2015-022 (2015)
[13] The ATLAS collaboration, ATL-PHYS-PUB-2015-015 (2015)
[14] http://atlas.web.cern.ch/Atlas/GROUPS/PHYSICS/PLOTS/JETM-2015-003/
[15] The ATLAS collaboration, ATL-CONF-2016-024 (2016)
[16] The ATLAS collaboration, ATL-PHYS-PUB-2016-014 (2016)
[17] The ATLAS collaboration, ATL-PHYS-PUB-2015-025 (2015)
[18] https://twiki.cern.ch/twiki/bin/view/AtlasPublic/TauPublicCollisionPlots#Performance_plots_for_LHCC_2015
[19] The ATLAS collaboration, Eur. Phys. J. **C76**, 292 (2016)